ELSEVIER

Contents lists available at ScienceDirect

# Chemical Engineering Journal

journal homepage: www.elsevier.com/locate/cej



# Flexible nonwoven ZrO<sub>2</sub> ceramic membrane as an electrochemically stable and flame-resistant separator for high-power rechargeable batteries



Panpan Jing<sup>a,b,1,\*</sup>, Mengting Liu<sup>b,1</sup>, Peifeng Wang<sup>a</sup>, Jun Yang<sup>a</sup>, Manjing Tang<sup>a</sup>, Chenpu He<sup>a</sup>, Yongping Pu<sup>a</sup>, Meilin Liu<sup>b,\*</sup>

- <sup>a</sup> School of Materials Science and Engineering, Shaanxi Key Laboratory of Green Preparation and Functionalization for Inorganic Materials, Shaanxi University of Science & Technology, Xi'an, Shaanxi Province 710021, PR China
- b School of Materials Science and Engineering, Georgia Institute of Technology, Atlanta, GA 30332, USA

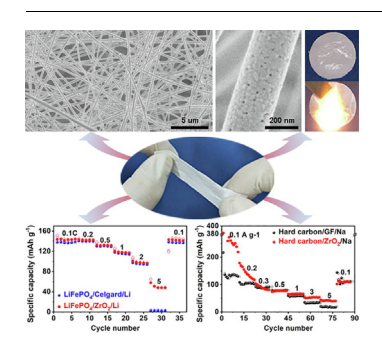
#### HIGHLIGHTS

- A ZrO<sub>2</sub> ceramic separator composed of nanofibers was fabricated via a simple route.
- The ZrO<sub>2</sub> membrane has remarkable mechanical flexibility and ample porosity.
- The ZrO<sub>2</sub> membrane has excellent flame-resistance and electrochemical inertness.
- The ZrO<sub>2</sub> membrane shows superior electrolyte wettability and ionic conductivity.
- The ZrO<sub>2</sub> separator can sustain higher current densities than commercial separators.

## ARTICLE INFO

Keywords:
Rechargeable Li<sup>+</sup> (Na<sup>+</sup>) battery
Full-inorganic separator
ZrO<sub>2</sub>
Flexible ceramic membranes
High power batteries

#### GRAPHICAL ABSTRACT



#### ABSTRACT

New-generation rechargeable batteries should not only have higher energy densities and faster rate capabilities than the exisiting ones, they should also be eco-friendly, low cost and safe. One of the most critical and enduring component of rechargeable batteries, the state-of-the-art polyolefin separators fail to perform sufficiently in several battery applications, notably those requiring high current densities and elevated temperatures. Herein, we report a nonwoven ZrO<sub>2</sub> ceramic membrane with a robust nanofiber microstructure via polymeric electrospinning followed by a high-temperature organic burn-off. The as-synthesized ZrO<sub>2</sub> membrane shows remarkable mechanical flexibility, ample porosity, excellent electrolyte wettability and infiltration, outstanding heat and flame-resistance, and high electrochemical inertness. When tested in a lithium or sodium battery, the ZrO<sub>2</sub> separator can withstand higher current densities and have longer cycling lives than the state-of-the-art separators. Therefore, the ZrO<sub>2</sub> membrane shown in the current work can be represented as a promising alternative separator for a new-generation of safe, high-power batteries.

<sup>\*</sup>Corresponding author at: School of Materials Science and Engineering, Shaanxi Key Laboratory of Green Preparation and Functionalization for Inorganic Materials, Shaanxi University of Science & Technology, Xi'an, Shaanxi Province 710021, PR China (P. Jing).

E-mail addresses: jingpanpan@sust.edu.cn (P. Jing), meilin.liu@mse.gatech.edu (M. Liu).

<sup>&</sup>lt;sup>1</sup> The auothers contributed equally to this work.

#### 1. Introduction

Rechargeable lithium batteries have been studied for decades, primarily for powering portable electronics, robotics and other wireless electronics due to their remarkably high specific and volumetric energy densities and competitive cycle life [1,2]. Recently, batteries have also been playing an increasingly important role in new emerging applications such as electrical grid load-leveling and commercially competitive electric vehicles [3,4]. When pushing batteries to their performance limits, notable safety issues such as fires and explosions can occur, especially at high current densities and elevated temperatures [5]. The nature of these failures is complicated and is often attributed to a combination of individual failures of several different components of the cell. One of the primary failure modes is shorting-circuiting between the anode and cathode due to the penetration of Li dendrites through the separator, which is accelerated at high current densities and elevated temperatures above 40 °C, which generally appears at the hot weather and special work environments, such as the peripheral position of the vehicle engines, of which the temperature can be reached at 75-80 °C [6,7]. While substantial research efforts are underway to mitigate the growth of these dendrites, a parallel effort should be undertaken to develop more robust separators, which is the goal of this current study.

The role of the separator in a battery is to electronically insulate the anode from cathode while allow for the free transport of ions. In this capacity, the separator can greatly influence the rate performance, cell life, and safety of batteries [8]. When designing a separator material, there are several things to consider: a separator must be chemically inert under both strong oxidizing and reducing conditions in an organic electrolyte solution, thermally stable over a wide range of temperatures, flame resistant, ionic conductive with an ionic transference number close to unity, highly porous to enable the free flow of ions through the separator but also tortuosity to block the growth of Li dendrites, absorbent to maintain wetting of the electrolyte and mechanically robust [9,10]. It is very difficult to design a separator that can fulfill all of these requirements, so different types of separators must be developed to satisfy different applications. To date, the most familiar commercially separators are Celgard separators that made of porous polyolefin films, such as polypropylene (PP), polyethylene (PE) or a mixture of these materials [10-12]. Due to their organic nature, however, polyolefin and related separators suffer from low porosity and serious thermal shrinkage at above mentioned high temperatures due to its low melting point, which both can compromise battery performance and safety over long periods of time [10-12].

Extensive research efforts have been devoted to construct inorganic/organic composite separators, such as hydroxyapatite/cellulose [10], SiO<sub>2</sub>/polyimide [13], Al<sub>2</sub>O<sub>3</sub>/PE [11,14], and others [15–19]. Although these separators have made strides in mediating the problems of high power density breakdown and electrolyte wettability/infiltration, they are still poor in terms of the thermal stability due to small percentages of remnant organic material. Also, because some separators are prepared by coating the inorganic particles on the surface of organic components by using binders, it is likely that these particles may become detached and contaminate the electrolyte after extended use. Thus, considerable efforts should be placed to develop full-inorganic separators to address these issues. ZrO2 is an eco-friendly and chemically inert refractory ceramic material that has been incorporated with an organic framework to function as a separator [20-22]. To the best of our knowledge, however, the pure material has never been reported for use as a separator due to its mechanical fragility.

Herein, a mass-producible pure ZrO<sub>2</sub> nonwoven membrane was prepared via a polymeric electrospinning route followed by organic material burnout. The synthesized membrane exhibits a remarkable flexibility, finely tailored porosity, high electrolyte wettability and infiltration, high thermal stability and flame-resistance, high ionic conductivity and electrochemical stability. When used as a separator for

Li<sup>+</sup> (Na<sup>+</sup>) batteries, the batteries outperformed traditional separators in terms of rate capability and cycle life. The ZrO<sub>2</sub> membrane represents a promising candidate to traditional separators for the next-generation of high-performance batteries, notably those that require high thermal stability and high power.

#### 2. Experimental details

#### 2.1. Synthesis of flexible ZrO<sub>2</sub> nonwoven membrane

The flexible ZrO<sub>2</sub> nonwoven membrane was synthesized by a polymeric electrospinning route followed by air-annealing to burnout organic materials. Firstly, a clear and viscous electrospun-sol was prepared by dissolving  $\sim 0.5$  g of polyvinylpyrrolidone (Mw = 1,300,000) powders in a 20 g of zirconium acetate solution under vigorous stirring for overnight. In order to enhance the flexibility and mechanical strength of the resulting ZrO2 nonwoven membrane, a little bit of stabilizer (yttrium nitrate) was added into the above sol. Next, a moderate amount of the as-obtained sol was transferred to a glass syringe as the reservoir of an electrospinning device and spun under a voltage of 20 kV. The apparatus was self-assembled in our lab using a syringe equipped with a stainless steel needle as the spinning jet, a high-voltage power supply, a micro-injection pump, a drum collector and a glass cover. The receiving distance, jet flow rate and pump rotating speed were set to 17 cm, 0.3 mL h<sup>-1</sup> and 20 rpm, respectively. To obtain a precursor nonwoven membrane possessing a sufficient thickness, at least 10 mL of sol must be used. After drying at 80 °C for about 24 h in a drying oven, thirdly, the collected nonwoven membrane precursor was followed by an annealing at 800 °C for 2 h. The heating and cooling rates was 5 °C min<sup>-1</sup>. Finally, the flexible ZrO<sub>2</sub> nonwoven membrane was then punched into the separators for the Li<sup>+</sup> (Na<sup>+</sup>) batteries.

#### 2.2. Material characterization

The phase purity and crystal structure of the ZrO2 nonwoven membrane were determined by using an X-ray diffractometer (XRD, Bruker Discover & Diffractometer, Cu Ka radiation). Field-emission scanning electronic microscopy (FE-SEM, Hitachi SU8010), Transmission electron microscopy (TEM, FEI Tecnai G2 F20) as well as high-resolution TEM (HRTEM) measurements were used to reveal the microstructural features of the ZrO2 nonwoven membrane. The pore size distribution and porosity were investigated by using a mercury porosimeter (AutoPore IV 9500). The Nitrogen adsorption-desorption data was also recorded to determine the specific surface area by using a Brunaur-Emmett-Teller surface analyzer (Gemini VII2390). Contact angle tests by using a JC2000C goniometer and thermogravimetry analysis (TGA) by using a SDT Q600 Instruments DSC-TGA under Air flow at the rate of 10 °C min<sup>-1</sup> were performed to investigate the electrolyte wettability and thermal stability of the ZrO2 nonwoven membrane, respectively. Electrochemical impedance spectroscopy (EIS) was recorded at room temperature to investigate the ionic conductivity of the ZrO2, which was soaked in the liquid LiPF6 electrolyte and sandwiched between two stainless steel plates with a 1.77 cm<sup>2</sup> area. The tests were performed over the frequency range of 10<sup>-2</sup> Hz to 100 Hz with an AC amplitude of 10 mV. The ionic conductivity (σ) was calculated using the following equation:  $\sigma = d/(R_b \cdot S)$ , in where d and R<sub>b</sub> refer to the thickness and bulk resistance of the separators, respectively, and S refers to the area of stainless steel plates. In order to check the electrochemical stability of ZrO2 separator, the linear sweep voltammetry (LSV) tests were carried out at the scan rate of 1 mV s<sup>-1</sup> by using the stainless steel/electrolyte-soaked separator/Li half-cell, in which lithium metal acted as counter electrode and stainless steel acted as working electrode. All the above mentioned EIS and LSV measurements were conducted at an electrochemistry working station equipped with a Solartron 1255 HF frequency response analyzer.

#### 2.3. Electrochemical measurement

In order to evaluate the practical applications of the ZrO<sub>2</sub> nonwoven membrane in Li<sup>+</sup> (Na<sup>+</sup>) battery, the membrane was punched into disc separators with a diameter of 18 mm and assembled into the 2032 cointype half-/full-cells in a glove box filled with argon. In the Li<sup>+</sup> half-cell configuration, Li foil was used as the anode, and the cathode was made by making of slurry of commercial LiFePO<sub>4</sub> (active material), PVDF (binder) and acetylene black (conductive agent) powders with a mass ratio of 8:1:1 in 1-methyl-2-pyrrolidone (NMP) and coated on Al foil was used as cathode. The mass loading was controlled at the range of 2-3 mg cm<sup>-1</sup>. The above cathode was also used in the Li<sup>+</sup> full-cell. where the anode was prepared by coating a slurry of the commercial hard carbon (active material) mixed with conductive agent and binder on an Al foil. 1 M LiPF<sub>6</sub> in a 1:1 mixture solvent of EC: DMC was used as the liquid electrolyte for both the Li+ half-/full-cells. In the Na+ halfcell configuration, besides the ZrO2 separator, Na foil, hard carbon and commercial NaClO<sub>4</sub> solution were respectively used as the cathode, anode active materials and electrolyte. The battery performance including discharge-charge curves and specific capacities at various rates (Li<sup>+</sup> battery: 0.1, 0.2, 0.5, 1, 2 and 5C; Na<sup>+</sup> battery: 0.1, 0.2, 0.3, 0.5, 1, 2 and 3 A  $\ensuremath{\text{g}^{-1}}\xspace$  ) and cycling performance were measured using a LAND-CT2001A battery testing system in the voltage window of 2.5-3.65 V (vs. Li<sup>+</sup>/Li) and 0.01–3.0 V (vs. Na<sup>+</sup>/Na), respectively. As references, the Li+ half-/full-cells using the commercial Celgard 2004 separator and Na+ half-cells using the commercial glass fiber were also assembled and tested.

#### 3. Results and discussion

Fig. S1a-f shows several digital photographs of the as-prepared ZrO<sub>2</sub> membrane in different states of fabrication. It can be clearly seen from Fig. S1a that the as-spun precursor membrane detached from the electrospinning drum collector (Fig. 1a) has a smooth surface. After firing the precursor membrane in air at 800 °C for 3 h, the membrane (Fig. S1b) well maintains the appearance of the defect-free precursor membrane, only decreasing slightly in size. When the membrane experiences hard bending and folding operations (Fig. S1c and d), the original structure was easily recovered, saving for a few fold creases (Fig. S1e). It is apparent through these tests that the membrane possesses an excellent flexibility and toughness. Furthermore, when a ribbon was cut from the membrane and pulled in tension, no notable tearing or ripping was observed (Fig. S1f). As seen in the corresponding insets, the membrane can easily be punched into suitable separators for coin cell fabrication while still maintaining flexibility and high mechanical strength. Fig. S2 shows the XRD pattern of the membrane. All diffraction peaks indicate high crystalline and match with those of cubic ZrO2 (JCPDS no. 49-1642) without any obvious impurity phases in the membrane. SEM and TEM images were taken to explore the microstructure and porosity of the ZrO2 membrane. As revealed in Fig. 1b, the membrane is composed of nanofibers stacked and connected in random orientations. The nanofibers are hundreds of microns in length and measure from 170 nm to 450 nm in diameter with an average diameter around 290 nm (Fig. 1b inset). The high magnification SEM image (Fig. 1c) reveals that the ZrO2 nanofibers are quite uniform along their long axis directions and their surfaces are filled with abundant pores. It is well known that this porous structure is due to the decomposition of PVP used in fiber formation and particle crystallization during heat treatment. The TEM image (Fig. 1d) confirms that the nanofibers are highly porous and are composed of interconnected particles around 20 nm. Fig. 1e shows an HRTEM image, in which the lattice fringes can be clearly observed for the nanofibers. Several lattice spacing were measured with values of 0.313 and 0.310 nm, corresponding to the (1 1 1) crystal plane of ZrO<sub>2</sub>. These measurements further verify that the ZrO2 nonwoven membrane is indeed phase pure and that the lattice is not strained in any way during

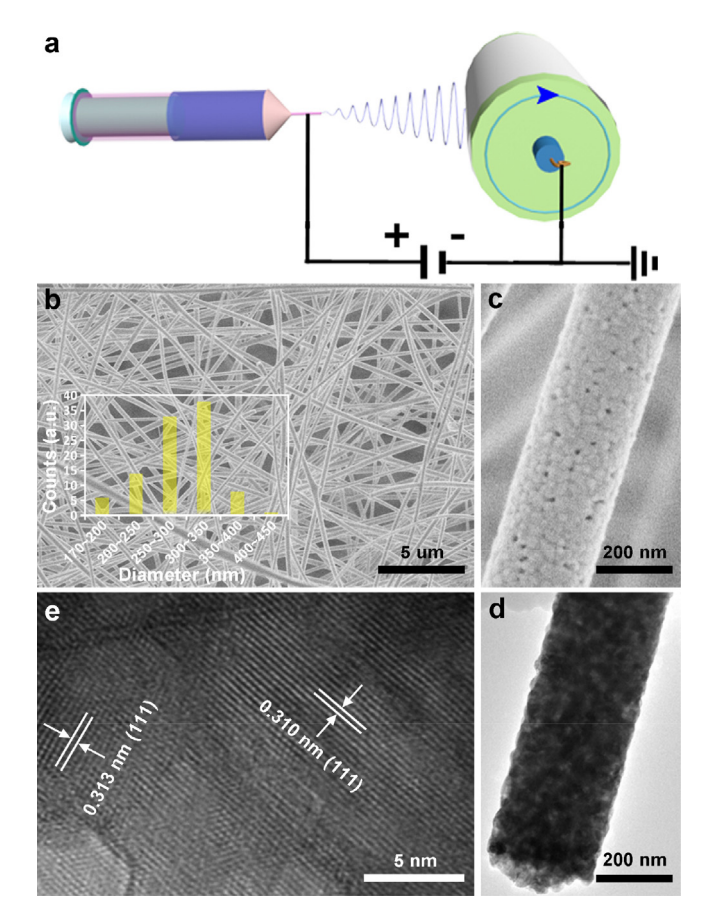


Fig. 1. a) Schematic of the electrospinning device. b, c) Low and high magnification SEM images, d) TEM and e) HRTEM images of the  ${\rm ZrO_2}$  membrane.

synthesis.

Fig. S3a and b show the evolutions of the contact angles of typical Li<sup>+</sup> electrolytes (LiPF<sub>6</sub>) with time on the as-punched ZrO<sub>2</sub> and commercial Celgard-2004 separators, which were ~50 μm and 25 μm thick, respectively. After placing the liquid LiPF<sub>6</sub> electrolytes onto the surface of the ZrO2 separator, the contact angle was initially only 11.5° and completely disappears after 0.05 s. However, the initial contact angle on the commercial Celgard separator was 35.9° and remained unchanged with a long time. Therefore, the ZrO2 separator shows excellent electrolyte wetting capability for Li+ electrolyte. To more clearly visualize this wetting phenomenon, the liquid electrolytes was dyed with a small amount of Rhodamine B dye and was dropped on the separators. As show Fig. 2a, the initial drops of dyed Li+ electrolyte immediately soaked and spread into the ZrO<sub>2</sub> separator. After 10 drops of electrolyte, the ZrO<sub>2</sub> separator was fully wet. When the separator was moved to the aside from the original position, a small amount of excess electrolytes was found underneath, indicating that the ZrO<sub>2</sub> separator can be easily penetrated. In stark contrast, the LiPF<sub>6</sub> electrolyte barely penetrated the Celgard separator, maintained its overall shape and gradually grew bigger with the increasing drops (Fig. 2b). Fig. 2c shows the recorded pore size distribution curves found using Mercury Porosimetry. It is clear to find that the ZrO2 separator has a more uniform pore size distribution than the Celgard separator. Moreover, the porosity of the ZrO<sub>2</sub> separator is as high as 63.45% and much higher than 38.42% of the Celgard separator. Fig. 2d displays the TG curves of the ZrO2 and commercial Celgard separators were tested from room temperature to 800 °C in air. It is seen that the Celgard separator (black curve) experienced up to 99% weight loss, while the ZrO2 separator (red curve) only experienced about 7.5% weight loss when the temperature was just raised to 600 °C. The slight weight loss for the ZrO<sub>2</sub> membrane is likely attributed to the evaporation of water molecules

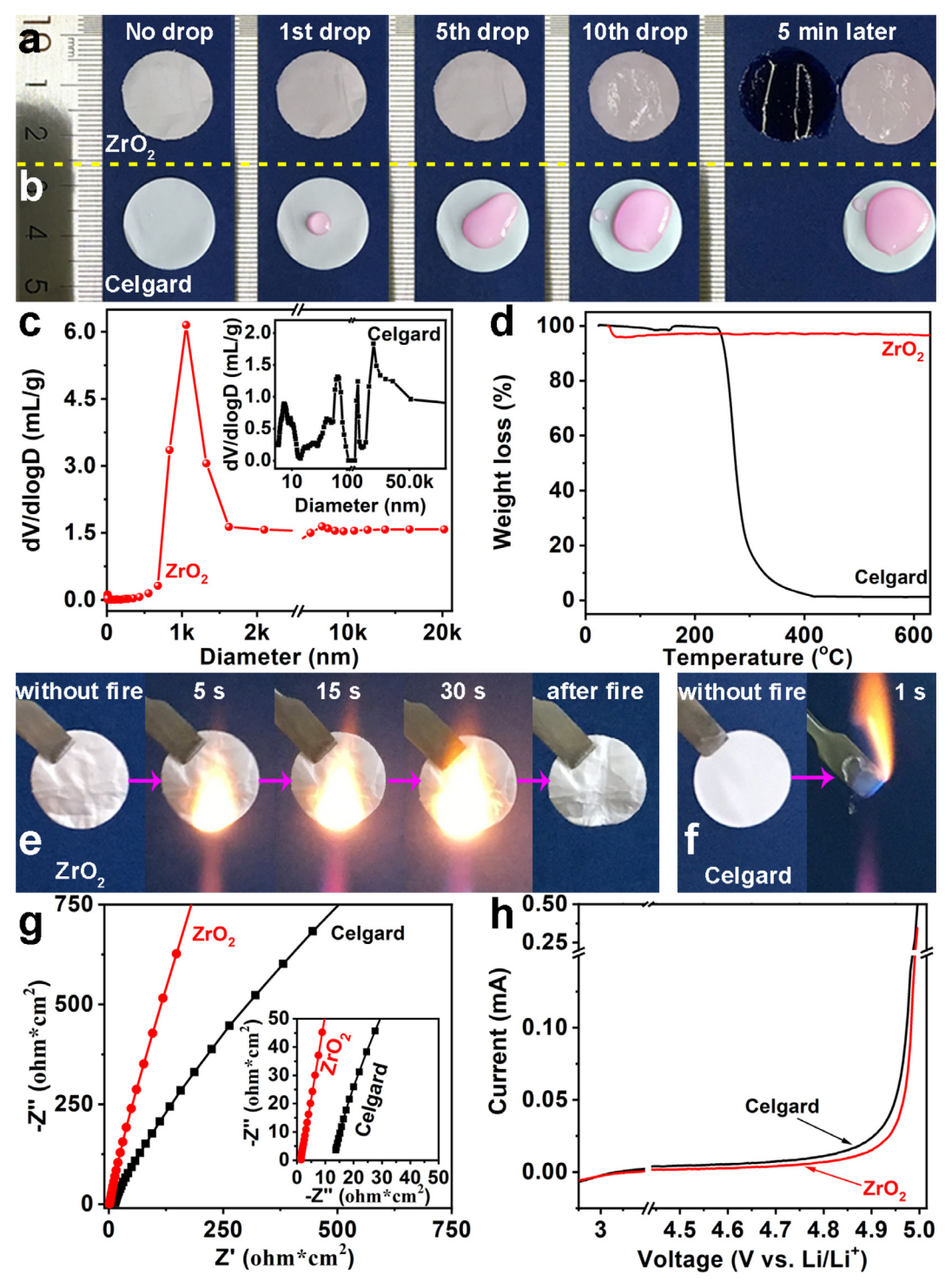


Fig. 2. (a, b) Digital photographs acquired from the ZrO<sub>2</sub> and Celgard separators after adding different drops of liquid LiPO<sub>6</sub> electrolyte dyed by a few Rhodamine B. (c) pore-size distribution curves, (d) TGA curves, (e, f) Fire-resistant tests of the ZrO<sub>2</sub> and commercial Celgard separators. (g) Nyquist plots of SS/separator/SS half-cells and (h) LSV curves of the SS/separator/Li half-cells using liquid LiPF<sub>6</sub> electrolyte soaked ZrO<sub>2</sub> and Celgard separators, respectively.

absorbed on the surface of separator. Furthermore, Fig. 2e and f show digital images of the interaction of each separator with a flame, respectively. The  $\rm ZrO_2$  separator (Fig. 2e) can't be lit and showed no apparent remarkable shrinkages after a 30 s flame exposure, while the Celgard separator (Fig. 2f) burned instantly. From these results, it is apparent that the  $\rm ZrO_2$  separator exhibits much better wettability and penetration with both  $\rm Li^+$  electrolyte as well as much greater thermal stability and fire-resistance than the commercial Celgard separator.

Ionic conductivity and electrochemical stability are two other

important performance metrics regarding separators for commercial use. In this work, the electrochemical impedance spectrum (EIS) and linear sweep voltammetry (LSV) were used to quantify these metrics for the ZrO<sub>2</sub> separator and commercial Celgard separator as a direct comparison. Fig. 2g shows the recorded Nyquist plots of the ZrO<sub>2</sub> (red curve) and Celgard (black curve) separators, which were fully wet with the liquid LiPF<sub>6</sub> electrolyte and placed between two stainless steel (SS) electrodes. The specific area resistance of the Celgard separator was found to be  $\sim$ 4.41  $\Omega$  cm<sup>-2</sup> but only 0.25  $\Omega$  cm<sup>-2</sup> for the ZrO<sub>2</sub>

separator. Using the Nyquist plots, the equivalent ionic conductivity of the electrolyte-soaked ZrO2 separator was calculated to be about 3.5 mS cm  $^{-1}$ , almost ten times great than that of the electrolyte-soaked Celgard separator (0.37 mS cm<sup>-1</sup>). Besides that, such excellent ionic conductivity of the ZrO2 separator is also higher than other reported separators, such as hydroxyapatite/cellulose (3.07 mS cm<sup>-1</sup>), [10]  $SiO_2$ /polyimide (2.27 mS cm<sup>-1</sup>), [13]  $Al_2O_3$ /PE (0.846 mS cm<sup>-1</sup>) [14] and others. It is apparent that the ZrO2 separator shows a much higher ionic conductivity due to the material's larger porosity and superior electrolyte wettability.[10,11,13,14] To record LSV curves, the LiPF<sub>6</sub> liquid electrolyte-soaked separators were assembled into half-cells by sandwiching them between a SS sheet as working electrode and Li metal as the counter and reference electrode. In the operation voltage window from 3.0 to 5.0 V, as shown in Fig. 2h, the Celgard separator begins to disintegrate at about 4.75 V while there are not any distinctive changes in the ZrO2 separator until at about 4.93 V, from which the current begains to increase gradually. This indicates that the ZrO2 separator has greater electrochemical inertness than the Celgard separator in addition to the numerous details discussed previously.

To evaluate the ZrO2 separator in a realistic application, it was

assembled into a LiFePO<sub>4</sub> half-cell with Li metal in the configuration of LiFePO<sub>4</sub>/separator/Li. Fig. 3a displays the initial discharge-charge profiles of the half-cell at different rates ranging from 0.1 to 5C, demonstrating an impressive rate capability. The specific capacity decreases accordingly with increasing the current density. All of the discharge and charge plateaus observed on the profiles are corresponds to the redox reactions of LiFePO<sub>4</sub> with Li<sup>+</sup>. Fig. 3b shows a comparison of the rate performance between the half-cells with the ZrO2 and commercial Celgard separators. One can see that the cell with the ZrO<sub>2</sub> separator exhibits a similar specific capacity as the cell with the Celgard separator when the current densities are below 0.83 mA cm<sup>-2</sup> (corresponding to 2C). When the current density increases to 2.08 mA cm $^{-2}$ (corresponding to 5C), there is a marked difference between the two cells, with the ZrO<sub>2</sub> separator delivering a capacity of 48 mAh g<sup>-1</sup> and the Celgard separator delivering almost no capacity (2.8 mAh/g), making it apparent that rate performance is not only dictated by the choice of the active electrode material but also by the choice of the separator. Under the same cell-configuration, the ZrO2 separator enables much higher rate capability and power density than the Celgard separator even it thickness is double, due to its greater diffusion-limited

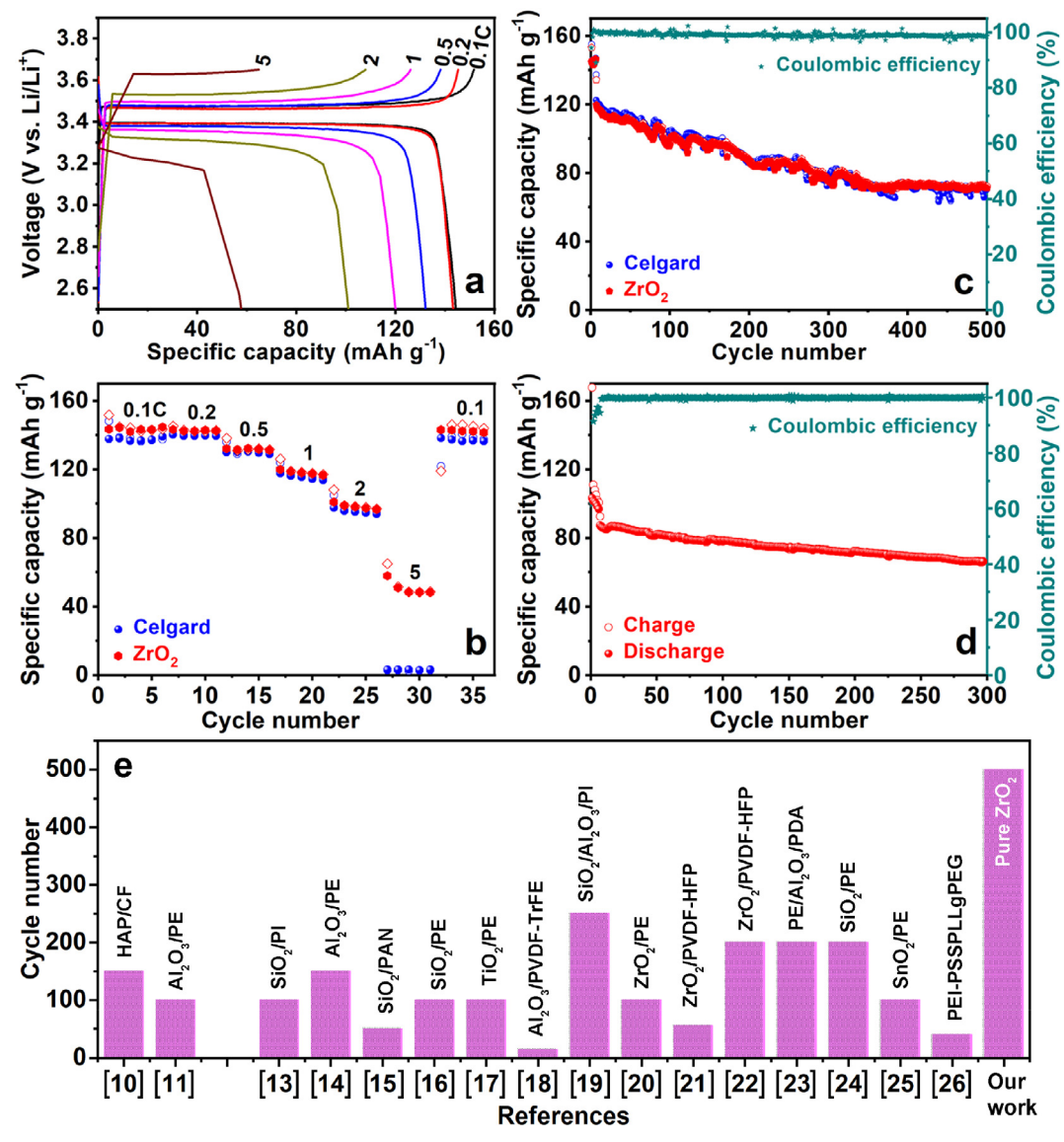


Fig. 3. (a) The initial discharge–charge profiles of the LiFePO $_4$ /ZrO $_2$ /Li half-cell at different rates. (b) Rate capabilities and (c) cycling stabilities of the LiFePO $_4$ /ZrO $_2$ /Li and LiFePO $_4$ /ZrO $_2$ /HC full-cell at 1C. (e) Cycling stability comparison of separators between our work and others.

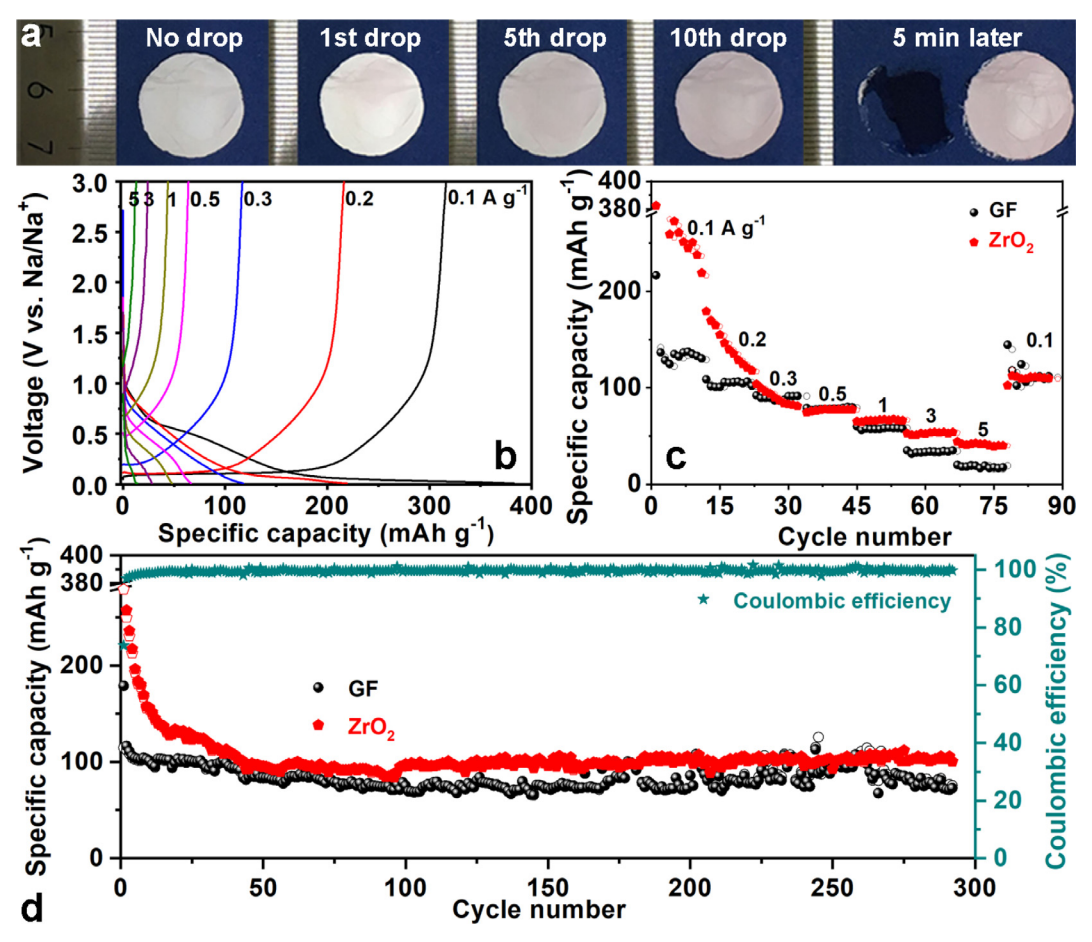


Fig. 4. (a) Digital photographs acquired from the  $ZrO_2$  separator after adding different drops of liquid  $NaClO_4$  electrolyte dyed by a few Rhodamine B. (b) Initial discharge–charge profiles of the  $Na/ZrO_2/HC$  half-cell at different current densities, (c) Rate capabilities and (d) cycling performance at 0.1 A  $g^{-1}$  of the  $Na/ZrO_2/HC$  and Na/GF/HC half-cells.

current density. As displayed in Fig. S4, we further revealed the rate performance of the battery with ZrO2 separator in thickness of ~134 µm. Similarly, the specific capacity decreases gradually with increasing the rates. Compared with the ZrO<sub>2</sub> separator in the thickness of 50 µm, interestingly, there is no remarkable changes of specific capacity under low rates even though the thickness is 134 µm. When the rate increased from the 1C to 5C, however, one can see that the specific capacity is decreased. It means that the thickness of ZrO2 separator has a significant effect on the high-rate performance of the battery, which can be ascribed to the decreased porosity and electrolyte wettability. Fig. 3c presents the cycling performance of the ZrO<sub>2</sub> and Celgard separator half-cells at a rate of 1C (or current density of 0.415 mA cm<sup>-2</sup>). The plots shows that both cells can reach a capacity of 71 mAh g<sup>-1</sup> for 500 cycles, but the ZrO<sub>2</sub> separator maintains greater stability over time. As shown in Fig. 3e, in our case, the 500 discharge-charge cycles is substantially greater than most organic/inorganic separators reported in literatures.[10,11,13-26] Moreover, the LiFePO<sub>4</sub>/separator/hard carbon (HC) full-cell was assembled and tested using the same current density of 1C to further verify the advantages of the ZrO<sub>2</sub> separator. As seen in Fig. 3d, the cell delivers an initial discharge (charge) specific capacity of 167 mAh g<sup>-1</sup> (120 mAh g<sup>-1</sup>). Although the first coulombic efficiency is only about 71.8%, the value increases rapidly to above 93% from the 2nd cycle and remains constant. After 300 cycles, the cell still delivers a considerable capacity of 66.3 mAh g<sup>-1</sup> with a high coulombic efficiency of 99.8%. Therefore, the ZrO2 membrane shows similar long term stability to the Celgard separator, but again shows substantially better rate performance.

For Na+ batteries, commercial glass fiber (GF) separator has been

the most commonly used for fabricating cells [27-29]. While it is known that the GF separators are more expensive, there is little working regarding chaper, higher-power and more durable separators developement until now. As shown in Figs. 4a and S3c, the Na<sup>+</sup> electrolyte (NaClO<sub>4</sub>) can also easily access the ZrO<sub>2</sub> separator even at a large thickness of ~250 µm. In this work, therefore, we demonstrate the feasibility of using ZrO2 separator for Na+ half-cells using a hard carbon (HC) as the anode and a Na metal as the cathode and reference. The rate capability and cycling performance were tested. Cells using GF separators were used for comparsion. Fig. 4a shows the initial discharge-charge profiles of the half-cell using ZrO2 separator at different cycling rates ranging from 0.1 to 3 A g<sup>-1</sup>, showing a reasonable rate capability. Fig. 4b compares the rate performance of two half-cells using ZrO2 and GF separators. Clearly, although the specific capacity of the cell with the  ${\rm ZrO}_2$  separator decreases gradually from the initial value of 380 mAh  $g^{-1}$  under the low current densities of 100 and  $200~\text{mA}~\text{g}^{-1}$ , the value is still much larger than that of the cell with a GF separator. Besides, the first coulombic efficiency of 82.6% for the battery with ZrO2 separator is much higher than that of 65.38% for the battery with GF separator. As we all known, the capacity loss for the first cycle is ascribed to the formation of the solid-electrolyte interphase (SEI) on the active materials to a certain extent [28,29]. In our case, hence, the high first coulombic efficiency menas that the ZrO<sub>2</sub> separator can effectively inhibate the SEI formation. When the current density is increased to 500 mA  $g^{-1}$ , the capacities of the cell with the ZrO<sub>2</sub> and GF separators remain unchanged. However, when the current density is further increased to 1 and up to 3 A g<sup>-1</sup>, the superior rate performance of the ZrO<sub>2</sub> separator far exceeds that of the GF separator. This result is

consistent with that of LIBs (Fig. 3b) and further confirms the remarkable rate capability of the ZrO2 separator for both Li + and Na + batteries. When the current density is brought back to 0.1 A g<sup>-1</sup>, the initial specific capacity of the cell with the ZrO2 separator can be recovered while that of the GF cell is unstable. Fig. 4c presents the cycling performances of the half-cells with ZrO2 and GF separators at a current density of 0.1 A g<sup>-1</sup>. For nearly 300 discharge-charge cycles, the cell with the ZrO2 separator can deliver a higher specific capacity and better cycling performance than the GF separator. From these results, it is apparent that the ZrO<sub>2</sub> membrane has more suitable porosity and Na<sup>+</sup> transport properties than the GF separator, allowing for the batteries' fabrication with a substantially improved rate performance and long term stability. Based on the evaluation of the basic properties of the ZrO<sub>2</sub> membrane, such as flammability, porosity and mechanical durability, as well as the evaluation of the membrane as a separator in Li+ and Na+ batteries as compared to commercial separators, the ZrO2 membrane confirms a promising alternative for new-generation batteries, notably for those requiring elevated temperature cycling and high power draw.

#### 4. Conclusions

In summary, we have successfully synthesized a highly pure  $\rm ZrO_2$  nonwoven nanofiber membrane with tunable thickness through a simple sol-assisted electrospinning method followed by organic material burnout. Systematic investigations revealed that the as-prepared  $\rm ZrO_2$  membrane is a mechanically and thermally stable and flame-resistant separator with remarkable flexibility, large porosity of 63.45%, excellent electrolyte wettability and infiltration, high ionic conductivity and suitable electrochemical inertness. When the  $\rm ZrO_2$  membrane was used as a separator in  $\rm Li^+$  ( $\rm Na^+$ ) batteries, both the batteries had better rate capability at high current densities and cycling life compared to commercial Celgard and GF separators. Our nonwoven  $\rm ZrO_2$  membrane represents a step towards the development of fully inorganic and robust ceramic separators for new-generation  $\rm Li^+$  ( $\rm Na^+$ ) battery development.

# **Declaration of Competing Interest**

The authors declare that they have no known competing financial interests or personal relationships that could have appeared to influence the work reported in this paper.

#### Acknowledgments

This work was financially supported by the National Natural Science Foundation of China (51702201, 21805179), Guangdong Innovative and Entrepreneurial Research Team Program (2014ZT05N200), US National Science Foundation (DMR-1742828), and Natural Science Foundation of Shaanxi Province (2018JQ5036).

#### Appendix A. Supplementary data

Supplementary data to this article can be found online at https://doi.org/10.1016/j.cej.2020.124259.

### References

- D. Di Lecce, R. Verrelli, J. Hassoun, Lithium-ion batteries for sustainable energy storage: recent advances towards new cell configurations, Green Chem. 19 (2017) 3442–3467.
- $\hbox{\cite[2]}\ \ M.\ Li,\ J.\ Lu,\ Z.\ Chen,\ K.\ Amine,\ 30\ years\ of\ lithium-ion\ batteries,\ Adv.\ Mater.\ 30$

- (2018) 1800561
- [3] G. Zubi, R. Dufo-López, M. Carvalho, G. Pasaoglu, The lithium-ion battery: state of the art and future perspectives, Renew. Sust. Energy Rev. 89 (2018) 292–308.
- [4] Z.P. Cano, D. Banham, S. Ye, A. Hintennach, J. Lu, M. Fowler, Z. Chen, Batteries and fuel cells for emerging electric vehicle markets, Nat. Energy 3 (2018) 279–289.
- [5] K. Liu, Y. Liu, D. Lin, A. Pei, Y. Cui, Materials for lithium-ion battery safety, Sci. Adv. 4 (2018) 9820.
- [6] Y. Zhu, J. Xie, A. Pei, B. Liu, Y. Wu, D. Lin, J. Li, H. Wang, H. Chen, J. Xu, A. Yang, C.-L. Wu, H. Wang, W. Chen, Y. Cui, Fast lithium growth and short circuit induced by localized-temperature hotspots in lithium batteries, Nat. Comm. 10 (2019) 2067.
- [7] K. Liu, D. Zhuo, H.-W. Lee, W. Liu, D. Lin, Y. Lu, Y. Cui, Extending the life of lithium-based rechargeable batteries by reaction of lithium dendrites with a novel silica nanoparticle sandwiched separator, Adv. Mater. 29 (2017) 1603987.
- [8] M.F. Lagadec, R. Zahn, V. Wood, Characterization and performance evaluation of lithium-ion battery separators, Nat. Energy 4 (2019) 16–25.
- [9] P. Arora, Z. Zhang, Battery separators, Chem. Rev. 104 (2004) 4419-4462.
- [10] H. Li, D. Wu, J. Wu, L.Y. Dong, Y.J. Zhu, X. Hu, Flexible, high-wettability and fireresistant separators based on hydroxyapatite nanowires for advanced lithium-ion batteries, Adv. Mater. 29 (2017) 1703548.
- [11] X. Jiang, X. Zhu, X. Ai, H. Yang, Y. Cao, Novel ceramic-grafted separator with highly thermal stability for safe lithium-ion batteries, ACS Appl. Mater. Interfaces 9 (2017) 25970–25975.
- [12] M. Tang, J. Yang, N. Chen, S. Zhu, X. Wang, T. Wang, C. Zhang, Y. Xia, Overall structural modification of a layered Ni-rich cathode for enhanced cycling stability and rate capability at high voltage, J. Mater. Chem. A 7 (2019) 6080–6089.
- [13] Y. Wang, S. Wang, J. Fang, L.-X. Ding, H. Wang, A nano-silica modified polyimide nanofiber separator with enhanced thermal and wetting properties for high safety lithium-ion batteries, J. Membr. Sci. 537 (2017) 248–254.
- [14] H. Jeon, D. Yeon, T. Lee, J. Park, M.-H. Ryou, Y.M. Lee, A water-based  ${\rm Al_2O_3}$  ceramic coating for polyethylene-based microporous separators for lithium-ion batteries, J. Power Sour. 315 (2016) 161–168.
- [15] M. Yanilmaz, Y. Lu, J. Zhu, X. Zhang, Silica/polyacrylonitrile hybrid nanofiber membrane separators via sol-gel and electrospinning eechniques for lithium-ion batteries, J. Power Sour. 313 (2016) 205–212.
- [16] X. Zhu, X. Jiang, X. Ai, H. Yang, Y. Cao, A highly thermostable ceramic-grafted microporous polyethylene separator for safer lithium-ion batteries, ACS Appl. Mater. Interfaces 7 (2015) 24119–24126.
- [17] X. Zhu, X. Jiang, X. Ai, H. Yang, Y. Cao, TiO<sub>2</sub> ceramic-grafted polyethylene separators for enhanced thermostability and electrochemical performance of lithiumion batteries, J. Membr. Sci. 504 (2016) 97–103.
- [18] K. Bicy, S. Suriyakumar, P. Anu Paul, A.S. Anu, N. Kalarikkal, A.M. Stephen, V.G. Geethamma, D. Rouxel, S. Thomas, Highly lithium ion conductive, Al<sub>2</sub>O<sub>3</sub> decorated electrospun P(VDF-TrFE) membranes for lithium ion battery separators, New J. Chem. 42 (24) (2018) 19505–19520, https://doi.org/10.1039/ C8NJ01907J.
- [19] X. Liang, Y. Yang, X. Jin, Z. Huang, F. Kang, The high performances of SiO<sub>2</sub>/Al<sub>2</sub>O<sub>3</sub>-coated electrospun polyimide fibrous separator for lithium-ion battery, J. Membr. Sci. 493 (2015) 1–7
- [20] J.K. Pi, G.P. Wu, H.C. Yang, C.G. Arges, Z.K. Xu, Separators with biomineralized zirconia coatings for enhanced thermo-and electro-performance of lithium-ion batteries, ACS Appl. Mater. Interfaces 9 (2017) 21971–21978.
- [21] M. Wang, X. Chen, H. Wang, H. Wu, X. Jin, C. Huang, Improved performances of Lithium-ion batteries with a separator based on inorganic fibers, J. Mater. Chem. A 5 (2017) 311–318.
- [22] W. Xiao, Y. Gong, H. Wang, J. Liu, C. Yan, Organic-inorganic binary nanoparticle-based composite separators for high performance lithium-ion batteries, New J. Chem. 40 (2016) 8778–8785.
- [23] J. Moon, J.Y. Jeong, J.I. Kim, S. Kim, J.H. Park, An ultrathin inorganic-organic hybrid layer on commercial polymer separators for advanced lithium-ion batteries, J. Power Sour. 416 (2019) 89–94.
- [24] W. Na, K.H. Koh, A.S. Lee, S. Cho, B. Ok, S.-W. Hwang, J.H. Lee, C.M. Koo, Binderless chemical grafting of  $SiO_2$  nanoparticles onto polyethylene separators for lithium-ion batteries, J. Membr. Sci. 573 (2019) 621–627.
- [25] Y. Xiang, W. Zhu, W. Qiu, W. Guo, J. Lei, D. Liu, D. Qu, Z. Xie, H. Tang, J. Li, SnO<sub>2</sub> functionalized polyethylene separator with enhanced thermal stability for high performance Lithium ion battery, ChemistrySelect 3 (2018) 911–916.
- [26] R. Zahn, M.F. Lagadec, M. Hess, V. Wood, Improving ionic conductivity and lithium-ion transference number in lithium-ion battery separators, ACS Appl. Mater. Interfaces 8 (2016) 32637–32642.
- [27] D. Kim, K. Zhang, M. Cho, Y.-M. Kang, Critical design factors for kinetically favorable P-based compounds toward alloying with Na ions for high-power sodium-ion batteries, Energy Environ. Sci. 12 (2019) 1326–1333.
- [28] M. Liu, P. Jing, T. Wang, X. Hou, M. Liu, Z. Sun, J. Li, D. He, Pseudocapacitive reaction enhanced porous Co0.85Se/N-doped carbon anodes for advanced sodiumion battery with high rate and capacity, Electrochim. Acta 321 (2019) 134643.
- [29] L. Yan, G. Chen, S. Sarker, S. Richins, H. Wang, W. Xu, X. Rui, H. Luo, Ultrafine Nb<sub>2</sub>O<sub>5</sub> nanocrystal coating on reduced graphene oxide as anode material for high performance sodium ion battery, ACS Appl. Mater. Interfaces 34 (2016) 22213.